Dyes and Pigments 235 (2025) 112580

Contents lists available at ScienceDirect

Dyes and Pigments

journal homepage: www.elsevier.com/locate/dyepig

PVP formulations of bis-cyclometalated iridium(III) complexes bearing β-modified porphyrin ligands: Characterization and photodynamic action on bladder cancer cells

Nuno M.M. Moura [a,*], Melani J.A. Reis [a], Carlos Lodeiro [b,c], M. Graça P.M. S. Neves [a], José A.S. Cavaleiro [a], Carlos F. Ribeiro [d,e], Rosa Fernandes [d,e,f], Ana T.P.C. Gomes [a,d,e,g,**]

[a] LAQV-REQUIMTE, Department of Chemistry, University of Aveiro, 3810-193, Aveiro, Portugal
[b] BIOSCOPE Group, LAQV-REQUIMTE, Chemistry Department, Faculty of Science and Technology, University NOVA of Lisbon, 2829-516, Caparica, Portugal
[c] PROTEOMASS Scientific Society, 2825-466, Costa da Caparica, Portugal
[d] University of Coimbra, Coimbra Institute for Clinical and Biomedical Research (iCBR), Faculty of Medicine, 3000-548, Coimbra, Portugal
[e] University of Coimbra, Faculty of Medicine, Institute of Pharmacology and Experimental Therapeutics, 3000-548, Coimbra, Portugal
[f] University of Coimbra, Center for Innovative Biomedicine and Biotechnology (CIBB), Coimbra, Portugal
[g] Universidade Católica Portuguesa, Faculdade de Medicina Dentária, Centro de Investigação Interdisciplinar em Saúde, 3504-505, Viseu, Portugal

ARTICLE INFO

Keywords:
Porphyrins
Iridium complexes
Photodynamic therapy
Photosensitizer
Cancer

ABSTRACT

Cancer stands as the second leading global cause of death, following heart disease. Considering the severe side effects revealed by some chemotherapeutics for tumor treatment and anticancer therapies, the scientific community is actively exploring more effective alternatives. Photodynamic Therapy (PDT) mediated by porphyrin-based photosensitizers (PS) has emerged as an attractive alternative to more conventional therapies. In this study, we incorporated bis-cyclometalated iridium(III) complexes featuring porphyrin-arylbipyridine ligands into poly(vinylpyrrolidone) (PVP) micelle. This integration resulted in photostable PVP-PS formulations with a remarkable capability to generate singlet oxygen. These formulations were also efficiently internalized by HT-1379 cells and due to these features, their photodynamic action against human bladder cancer cells (HT-1376 cell line) was assessed. All the formulations demonstrated high photodynamic activity, with **PVP-2** and **PVP-3** proving to be the most promising PS, as evidenced by their lower $IC50_{PDT}$ values. It was also demonstrated that all PVP-based formulations provide a safe and effective approach for photodynamic therapy (PDT) in bladder cancer, as no cytotoxic effects were observed in Vero cells.

1. Introduction

Cancer is one of the leading causes of death worldwide and arises from the transformation of normal cells into tumor cells in a multi-stage process that typically advances from a pre-cancerous lesion to a malignant tumor [1]. Conventional cancer treatments, including radiotherapy, chemotherapy, and surgery, are facing increasing restrictions due to their severe side effects, risk of relapse, and high toxicity [2,3]. The search for effective, selective, specific, low-toxicity, and low-side-effect treatments/drugs has become one of the most critical goals in cancer treatments.

Since the approval of cisplatin by the Federal Drug Administration for solid tumor treatment in the 1970s, platinum-based drugs have emerged as one of the most widespread chemotherapeutic approaches for tumor treatments [4,5]. While these metallodrugs exhibit a good therapeutic effect on many tumors, their therapeutic value is accompanied by several side effects, such as neurotoxicity, nephrotoxicity, weakening of the immune system, and risk of reinfection. Additionally, the intrinsic or acquired resistance of cancer cells to these non-selective metallodrugs is limiting their application in cancer therapy [5–9].

Researchers have dedicated significant efforts to overcome the drawbacks associated with platinum-based drugs and to discover more selective and target-specific anticancer drugs to eradicate platinum-based drugs' side effects [7–10]. Other transition metal-based complexes have attracted the attention of the worldwide scientific community due to their appealing properties; among them are the

* Corresponding author.
** Corresponding author. LAQV-REQUIMTE, Department of Chemistry, University of Aveiro, 3810-193, Aveiro, Portugal.
E-mail addresses: nmoura@ua.pt (N.M.M. Moura), apgomes@ucp.pt (A.T.P.C. Gomes).

https://doi.org/10.1016/j.dyepig.2024.112580
Received 3 October 2024; Received in revised form 29 November 2024; Accepted 1 December 2024
Available online 8 December 2024

cyclometalated iridium-based complexes.

Cyclometalated iridium(III) complexes show suitable photophysical properties, including high emission quantum yields, high emission lifetimes, large Stokes shift, due to low-lying metal-to-ligand charge transfer (^{3}MLCT) transition, fairly long phosphorescence lifetimes, excellent stability and electroluminescent performance [11–14]. As a result, cyclometalated iridium(III) complexes have attracted great attention from researchers in several fields for decades. These complexes have found applications in diverse fields such as (photo)catalysis, photoelectrochemistry, electron transfer arrays, and as components in organic light-emitting diodes (OLEDs) devices [13,15–20]. Recently, research on cyclometalated iridium(III) complexes experienced significant growth in the field of medicinal sciences as a result of their appealing physicochemical, photophysical, and pharmacokinetic features. The potential of these type of complexes in bio-imaging, bio--sensing, and as anticancer drugs has been accessed, and their relative inertness, allowing the active molecule to reach successfully the desired target is considered an important advantage [1,11,21–25].

Photodynamic Therapy (PDT) has been gaining significance in cancer treatment due to its improved selectivity and efficacy. It is a promising approach to defeat conventional cancer treatment weaknesses, such as restricted applicability, lack of specificity, radiation damage, and severe side effects [26,27]. PDT is a non-invasive therapeutic procedure based on the light-triggered reaction of a photosensitizer (PS) with triplet oxygen ($^3O_2$), which leads to the generation of reactive oxygen species (ROS). After photoactivation at a specific wavelength, the PS reaches an excited singlet state and by intersystem crossing an excited triplet state. Then, the ROS generation mechanism can follow two different pathways: 1) Type I, which involves an electron transfer process to $^3O_2$ producing superoxide anions ($O_2^{\cdot-}$), hydroxyl radicals (OH), and hydrogen peroxyde (H_2O_2), and/or 2) Type II, where cytotoxic singlet oxygen ($^1O_2$) is generated as a result of a transfer of energy between the excited PS and the surrounding $^3O_2$. Type II mechanism has been pointed out as the prevalent process [26,28–30]. Such PDT approach requires the use of a non-toxic PS which is only activated by certain types of light irradiation which minimizes the systemic toxicity, improves the selectivity towards cancer cells, and precludes the development of drug resistance even after being applied repeatedly [31,32]. Furthermore, PDT can be combined with other anticancer therapies (*e.g.* surgery, chemotherapy, or radiotherapy), enhancing the potential applications of this technique [33,34].

Tetrapyrrole-based PS, such as porphyrins and related macrocycles (*e.g.* chlorins, bacteriochlorins, or phthalocyanines), constitute the most extensively studied group of PS due to their structural, chemical, photophysical, and photochemical features [35–38] Over the past few decades, synthetic porphyrins, namely *meso*-tetraarylporphyrins, were synthesized and modified to fine-tune their features, affording new derivatives suitable for diverse applications across various fields, including chemosensing [39–41], water remediation [42–44], (photo)catalysis [45–49], light-harvesting systems [50–54], bioimaging [55,56] and other biomedical aplications [57–65].

The modification of the *meso*-positions within a porphyrin core with active metal centers, using transition metal ions, like Re, Pt, Ir, or Ru, has attracted the interest of the scientific community, mainly by targeting the development of new (photo)catalysts, PS or photoluminescent compounds [27,66–69]. However, to the best of our knowledge, much less attention has been paid to the use of porphyrin-based PS iridium complexes coordinated at β-pyrrolic positions. To date, the only reported example is our recent study, where we evaluated the PS activity of porphyrin derivatives bearing attached ruthenium or iridium terpyridine units against resistant melanoma cells [70].

In this paper, the cellular internalization and photosensitizer ability of porphyrinic bis-cyclometalated iridium(III) complexes (**1**–**3**) were evaluated. The study was carried out on human bladder cancer cells (HT-1376 cell line) after incorporating the complexes into poly(vinylpyrrolidone) (PVP) micelles. The safety of the formultions was also evaluated using Vero cells.

2. Materials and methods

2.1. General remarks

The UV–Vis spectra were recorded on a UV-2501 PC Shimadzu spectrophotometer using DMF as solvent. Fluorescence emission spectra were recorded on a Horiba Jobin-Yvon Fluoromax 3 spectrofluorometer, and fluorescence quantum yields of PVP-PS formulations **PVP-1**, **PVP-2**, and **PVP-3** were measured by using a solution of 5,10,15,20-tetraphenylporphyrin (TPP) in DMF as a standard ($\Phi_F = 0.11$) [71].

2.2. Synthesis of Iridium(III) complexes 1–3

Porphyrinic bis-cyclometalated iridium(III) complexes **1**–**3** were synthesized according to the previous procedures described. The structures of both porphyrin-based PS were confirmed by ^{1}H NMR spectroscopy and mass spectrometry, and the data are in accordance with the data reported (ESI, Figs. S1–S24) [72].

2.3. General procedure to prepare PVP-PS micelles

Chloroform solutions of *N*-vinylpyrrolidone (VPD) (100 mg) and iridium(III)-based complexes **1**–**3** (10 % w/w) were mixed in a beacker and the solution stirred for 2 h at room temperature for a full homogenization. Then, the solvent was evaporated under nitrogen flow and the reddish-brown solid obtained was dried in an oven at 40 °C for 48 h. The resulting residues were dissolved in 2 mL of water and submitted to dialysis (using a membrane with a cutt-off of 12000 Da) in distilled water at pH 7, ensuring the complete elimination of organic solvents. After this approach, **PVP-1**, **PVP-2** and **PVP-3** formulations were obtained.

2.4. Photostability assays

In a glass cuvette PBS solutions of PVP-based formulations **PVP-1**, **PVP-2**, and **PVP-3** (5.0 μM) were prepared and kept in the dark at room temperature. Then such solutions were irradiated with white light (400–750 nm) using a light emission diode (LED) system (ELMARK – VEGA20, 20 W, 1400 lm) with an irradiance of 25 mW cm^{-2} for 30 min. The absorption spectra were recorded at 0, 1, 2, 3, 4, 5, 10, 20, and 30 min after irradiation.

2.5. Singlet oxygen generation

To evaluate the ability of PVP formulations (**PVP-1**, **PVP-2**, and **PVP-3**) to generate singlet oxygen ($^1O_2$), in a 1 × 1 cm glass cuvette were prepared 3 mL solutions containing each PS (0.5 μM) and 1,3-diphenylisobenzofuran (DPiBF) (50 μM) in DMF. The solutions were irradiated with a red-light LED board (630 ± 20 nm) at an irradiance of 11 mW cm^{-2} for 15 min at room temperature under gentle magnetic stirring. Control assays were performed using just a solution of DPiBF (50 μM) in DMF and solutions containing a DPiBF solution at 50 μM plus the formulations **PVP** or **PVP-TPP** (with **TPP** used as the standard; $\Phi_\Delta = 0.64$ in DMF [73]) at 0.5 μM.

2.6. Cellular uptake of PVP-PS formulations

The efficiency of cell uptake of **PVP-1**, **PVP-2** and **PVP-3** formulations was carried out using a human bladder cancer cell line HT-1376 derived from high-grade transitional cell carcinoma (from the American Type Culture Collection, ATCC, Manassas, VA, USA). This cell line was cultured in Roswell Park Memorial Institute medium (RPMI-1640) supplemented with 10 % (v/v) of fetal bovine serum (Life Technologies, Carlsbad, CA, USA), 100 U/mL penicillin, 100 mg/mL streptomycin and

0.25 mg/mL amphotericin B (Sigma).

HT-1376 cells were seeded (9.4×10^4 cells.cm^{-2}) in 96-well cell culture plates and maintained in the culture medium under an air atmosphere containing 5 % CO_2. For time- and concentration-dependent studies of the cell uptake, after seeding the cells overnight, they were washed twice with PBS and incubated for 2 h and 4 h in darkness (at 37 °C under an air atmosphere containing 5 % of CO_2) with **PVP-1**, **PVP-2** and **PVP-3** at 2.5, 5.0, 10.0 and 12.5 μM concentrations prepared in PBS. HT-1376 cells were immediately washed with PBS and lysed in 1 % m/v sodium dodecyl sulfate (SDS; Sigma) in PBS. **PVP-1**, **PVP-2** and **PVP-3** intracellular concentration was determined by spectrofluorometry using a microplate reader Synergy HT, BioTek, Winooski, VT, USA, equipped with excitation/emission wavelengths set of 360 nm/675 nm. The results were normalized for protein concentration (determined by bicinchoninic acid reagent; Pierce, Rockford, IL, USA).

2.7. In vitro cancer cytotoxicity after PDT treatment with PVP-PS formulations

The phototoxic effect of **PVP-1**, **PVP-2**, and **PVP-3** formulations was evaluated using the 3-[4,5-dimethylthiazol-2-yl]-2,5-diphenyl-tetrazolium bromide (MTT) assay. HT-1376 cells were seeded and treated with the different concentrations of **PVP-1**, **PVP-2**, and **PVP-3** formulations, as mentioned above, for 4 h in the dark. After the treatment, the cells were washed twice with PBS and covered with 100 μL of fresh medium. Cells were irradiated for 40 min with white light delivered by an illumination system (LC-122 LumaCare, London) equipped with a halogen/quartz 250 W lamp coupled to the selected interchangeable optic fiber probe (400–800 nm) at a fluence rate of 20 mW cm^{-2}. After 24 h of the PDT protocol, cell phototoxicity was determined by measuring the ability of cancer cells to reduce MTT (Sigma) to a colored formazan. The absorbance at 570 nm wavelength was measured using a microplate reader (Synergy HT, Biotek, Winooski, VT, USA). The data were expressed in percentage of control (i.e., the optical density of formazan from cells not exposed to PVP-PS formulations). The dark toxicity of **PVP-1**, **PVP-2**, and **PVP-3** formulations was evaluated under the same protocol, though without the irradiation procedure.

2.8. In vitro cytotoxicity of PVP formulations in Vero Cells

Cytotoxicity assessments of PVP-based formulations were performed using the Vero cell line (ECACC 88020401, African Green Monkey Kidney cells, GMK clone) following the guidelines outlined by the International Organization for Standardization (ISO 10993-5) [74]. The Vero cells were cultured in Dulbecco's Modified Eagle Medium (DMEM, Gibco BRL, Invitrogen), containing 10 % (v/v) fetal bovine serum (FBS, Gibco BRL, Invitrogen), along with 100 U/mL penicillin, 100 mg/mL streptomycin, and 0.25 mg/mL amphotericin B (Gibco BRL, Invitrogen).

Cells were plated at a density of 9.4×10^4 cells.cm^{-2} in 96-well cell culture plates and incubated at 37 °C under an air atmosphere containing 5 % of CO_2. Following two PBS washes, the cells were then incubated with DMEM solutions of **PVP-1–3** at concentration of 2.5, 5.0, 10.0 and 12.5 μM for 24 h under the same conditions. Cell viability was evaluated after incubation by measuring the ability of the Vero cell's to reduce resazurin (7-hydroxy-3*H*-phenoxazin-3-one-10-oxide sodium salt, Sigma) to resorufin, utilizing a microplate reader (SynergyTM HT Multi-Detection Microplate Reader-Biotek®) [75]. The viability results were expressed as a percentage relative to control cells [i.e., the optical density of resorufin (OD 570 nm) from cells not exposed to PVP formulations (Ct)].

2.9. Statistical analysis

The biological assays results are presented as the mean of at least 3 independent assays with 3 replicates per assay. The statistical analysis was performed with GraphPad Prism (GraphPad Software, San Diego, CA, USA). Statistical significance among the conditions was assessed using the nonparametric Mann-Whitney test.

3. Results and discussion

3.1. Synthesis

Mononuclear heteroleptic porphyrin-iridium(III) complexes **1**–**3** (Fig. 1) were synthesized by following a literature procedure [72]. Succinctly, the appropriate β-arylbipyridine porphyrin derivative was reacted with archetypal $[(ppy)_2Ir(bpy)][PF_6]$ complex in methanol. The reaction mixture was heated for 2 h at 120 °C in a sealed tube, followed by cooling to room temperature. Subsequently, an excess of an aqueous solution of KPF_6 was added. The resulting precipitate was filtered and washed consecutively with water and diethyl ether. After purification through column chromatography and crystallization in CH_2Cl_2/MeOH, the porphyrin-iridium(III) complexes **1**–**3** were obtained in yields ranging from 93 % to 96 %. The structural characterization of the porphyrinic bis-cyclometalated iridium(III) complexes **1**–**3** was conducted using UV–Vis, ^{1}H NMR and mass spectrometry, and all the experimental data agree with the described literature data (ESI, Figs. S1–S24) [72].

3.2. Incorporation into PVP micelles

Pursuing our interest in developing new porphyrin-based photosensitizers and motivated by the appropriate photophysical and photochemical properties displayed by porphyrin-iridium complexes **1**–**3** [72], we undertook the assessment of their photodynamic activity against cancer cells. However, owing to their low hydrophilic character (miLog *P*: 10.62–10.65) [76], it was mandatory to develop a strategy to overcome this drawback.

To enhance the hydrophilicity of the porphyrin-iridium complexes **1**–**3**, they were incorporated into poly(vinylpyrrolidone) (PVP) micelles. PVP is a synthetic water-soluble polymer obtained from *N*-vinylpyrrolidone (VPD), possesses unique properties applicable across various industries, ranging from food and cosmetic to pharmaceutical [77,78]. Among the several features of PVP-based formulations, inertness, non-toxicity, temperature- and pH-stability, and biocompatibility render it a versatile excipient for controlled or targeted delivery systems. Additionally, studies on the pharmacokinetic and pharmacological properties of PVP formulations reported a high affinity for both hydrophilic and hydrophobic drugs, as well as a significant enhancement in water-solubility and stability of the incorporated drugs [77–80].

Due to their versatility and stability, PVP formulations have already proven effective in solubilizing hydrophobic porphyrin-based PS in aqueous media, thereby improving PDT outcomes [81–84]. Furthermore, it was already reported in the literature the lack of cytotoxicity of PVP-based micelles for both normal and cancer cells after PDT treatment [84]. Recently, we described the incorporation of benzoporphyrin derivatives bearing (2,2′-bipyridine)dichloroplatinum(II) moieties into such micelles and the evaluation of their PS properties as PDT agents [10]. However, to the best of our knowledge, this approach has not yet been applied to *beta*-modified porphyrin-iridium(III)-type complexes.

The incorporation of each porphyrin-iridium(III) complexes **1**–**3** into PVP micelles represents a cost-effective approach involving the dissolution of both the PS and VPD in $CHCl_3$. The resulting solution was stirred for 2 h at room temperature, and then the solvent was removed under a nitrogen flow. The resulting residue, after being maintained for 48 h at 40 °C, was dissolved in water and subjected to dialysis, affording the expected PVP-PS formulations **PVP-1**, **PVP-2** and **PVP-3** through the quantitative encapsulation of the corresponding porphyrin-iridium(III) complexes **1**–**3**. The resultant PVP-formulations, as well as the unloaded PVP formulation for comparison purposes, underwent physical characterization (Table 1).

The self-assembled PVP solutions demonstrated uniformity, indicating their effective dispersion in water. Dynamic light scattering (DLS)

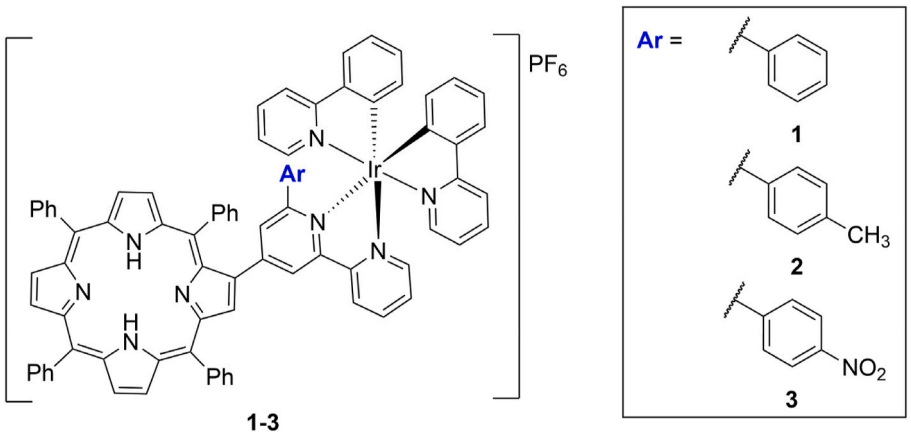

Fig. 1. Structures of porphyrin-iridium(III) complexes **1**–**3**.

Table 1
Physical characterization of PVP formulations in water.

PVP formulation	Hydrodynamic size (nm) ± SD	Polydispersity index (PDI) ± SD	*Zeta Potential (mV) ± SD*
PVP	88.8 ± 20.6	0.17 ± 0.02	−11.8 ± 0.5
PVP-1	101.5 ± 0.20	0.28 ± 0.01	10.0 ± 1.57
PVP-2	75.0 ± 0.21	0.20 ± 0.00	7.34 ± 0.35
PVP-3	106.2 ± 1.14	0.32 ± 0.01	7.69 ± 1.82

analysis shows that the PS-unloaded PVP formulation had an average hydrodynamic diameter of 88.8 nm. On the other hand, **PVP-1**, **PVP-2**, and **PVP-3** exhibited average particle sizes of 101.5 nm, 75.0 nm, and 106.2 nm, respectively (see Table 1 for details).

The incorporation of porphyrin-iridium(III) complexes **1** and **3** into PVP resulted in formulations with a slightly larger size than that of the unloaded particles. Among the loaded formulations, porphyrin-iridium (III) complex **2** afforded a more compact core, probably due to the slight higher hydrophobic nature of complex **2**, induced by the methyl group at the arylbipyridine moiety. Polydispersity index (PDI) values, obtained from DLS measurements and listed in Table 1, indicated that all formulations had acceptable PDI values, ranging from 0.20 to 0.32, slightly higher than those obtained for the unloaded PVP particles (0.18). This suggests the formation of a homogeneous and monodisperse population of PVP-based particle solutions, meeting the commonly acceptable practice threshold (≤0.3) for polymer-based nanoparticle materials used as drug delivery systems [85]. Zeta potential measurements in aqueous suspensions were employed to assess the surface charge of all PVP formulations. While the surface of PS-unloaded PVP micelle was negatively charged (ζ = −11.8 ± 0.5 mV), the incorporation of the porphyrin-iridium(III) complexes **1**–**3** into PVP-based micelles resulted in significant changes. The presence of porphyrin derivatives led to a reverse of the surface charge of PVP-formulations, mainly due to the cationic character of the $[Ir(bpy)(ppy)_2]^+$ moiety. Porphyrin-iridium (III) derivative **1** yielded the PVP formulation with a positively charged surface of ζ 10.0 ± 1.57 mV, while bis-cyclometalated iridium(III) complexes **2** and **3** induced a slightly lower positive surface charge of the corresponding PVP formulation with a value around ζ 7.5 mV.

The combination of appropriate size, homogeneous population, and a positively charged surface makes PVP-based formulations attractive carriers for PS **1**–**3**, especially in PDT applications to reduce the viability of cancer cells. These positive zeta potentials might be advantageous, given the negatively charged surface of cancer cells induced by the conversion of glucose to lactate through aerobic glycolysis [86]. This could enhance the interaction of PVP-based formulations with target cancer cells and facilitates PS release. Additionally, the size of PVP micelles prevents elimination through the kidneys, as observed for particles with sizes up to 10 nm, and avoids clearance by liver and spleen, which typically remove particles larger than 200 nm [87,88].

The photophysical characterization of each PVP-PS formulations was recorded in *N,N*-dimethylformamide (DMF) solution at 298 K. In general, it was observed that PVP-based formulations **PVP-1**, **PVP-2**, and **PVP-3** retained the photophysical features of the iridium(III) porphyrin complexes exhibiting analogous absorption, steady-state fluorescence emission, and excitation spectra, as well as fluorescence quantum yields.

The absorption spectra of the PVP-based micelles containing iridium (III) complexes **1**–**3** displayed the typical profile of *meso*-tetraarylporphyrin derivatives. However, upon comparison with the non-incorporated iridium(III) complexes **1**–**3** [72], it was observed that the absorption spectra were slightly red-shifted (3–5 nm) after incorporation into PVP micelles (Table 2 and Fig. 2). The PVP-based micelles exhibited a highly intense Soret band around 422 nm and four weak Q-bands ranging from 518 nm to 654 nm, typical from free-base *meso*-tetraarylporphyrin derivatives [89–91]. As expected, the UV–Vis spectra of the **PVP-1**, **PVP-2**, and **PVP-3** micelles confirmed that the iridium(III) complexation took place at the bipyridine moiety in β-pyrrolic position. Furthermore, no noticeable changes were observed after the incorporation of iridium(III) complexes into PVP-based micelles. A similar behavior was observed in the fluorescence emission spectra of PVP micelles, which displayed two emission bands at around 665 nm and 720 nm.

The excitation spectra for the as-prepared PVP-based formulations were also recorded. The observed resemblance with the corresponding absorption spectra confirmed the absence of emissive impurities. For PVP-PS formulations, was assessed the fluorescence quantum yield (Φ_F)

Table 2
Photophysical data of PVP-PS formulations **PVP-1**, **PVP-2** and **PVP-3** in DMF at 298 K.

Compd	λ_{max}(nm): log ε	λ_{em} (nm)	Stokes Shift (cm^{-1})	Φ_F
PVP-1	422:5.14 518:3.97 554:3.55 594:3.42 651:3.38	665, 721	3233.9	0.05
PVP-2	422:5.21 518:4.03 554:3.61 594:3.46 652:3.39	664, 721	2771.8	0.06
PVP-3	423:5.29 519:4.11 553:3.65 594:3.54 654:3.54	665,721	2529.3	0.07

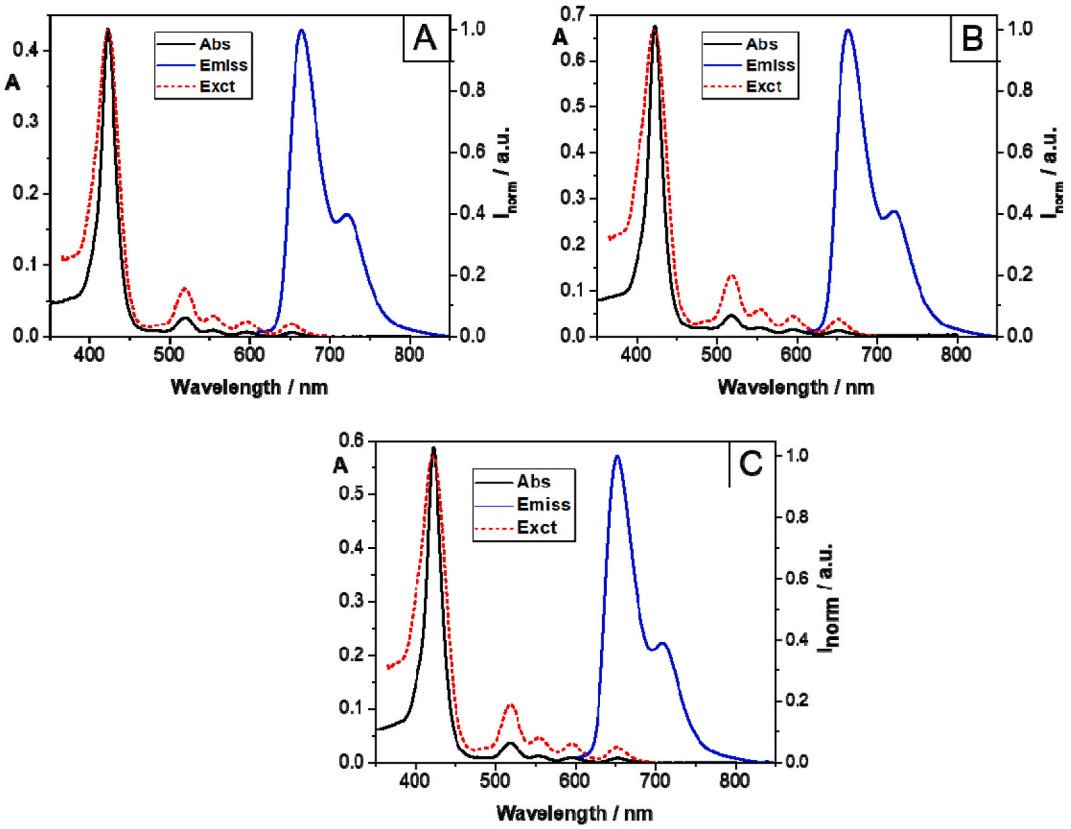

Fig. 2. Absorption (Abs) and normalized emission (Emiss) and excitation (Exct) spectra of PVP-PS formulations **PVP-1** (A), **PVP-2** (B) and **PVP-3** (C) in DMF at 298 K ([**PVP-1**] = [**PVP-2**] = [**PVP-3**] = 3.0 × 10^{-6} M; $\lambda_{ex\mathbf{PVP\text{-}1}} = \lambda_{ex\mathbf{PVP\text{-}2}} = \lambda_{ex\mathbf{PVP\text{-}3}}$ = 594 nm; $\lambda_{em\mathbf{PVP\text{-}1}} = \lambda_{em\mathbf{PVP\text{-}2}} = \lambda_{em\mathbf{PVP\text{-}3}}$ = 721 nm).

employing the internal reference method [92,93], with **TPP** ($\Phi_F = 0.11$) as reference [71,94,95]. After incorporation into PVP micelles, the porphyrinic-iridium(III) complexes **1**–**3** exhibited fluorescence quantum yields ranging from 0.05 to 0.07.

The incorporation of the porphyrinic bis-cyclometalated iridium(III) complexes **1**–**3** into PVP micelles did not induce considerable changes in their photophysical features. So, considering this, and the findings from a previously reported study where complexes **1**–**3** demonstrated high efficiency for use in photoinduced and photodynamic processes [72], prompted us to access if this potential as photosensitizer agents is maintained in such PVP- formulations.

3.3. Photostability and singlet oxygen generation

Both the photostability and the exceptional capacity of the porphyrinic-iridium(III) complexes **1**–**3** to generate $^1O_2$ [72] were assessed to determine whether their integration in PVP changed these two critical characteristics for a molecule to be employed in a PDT setting. In general, $^1O_2$ is recognized as the main cytotoxic species responsible for causing cell damage and consequent reductions in cell viability. Since low stability during light irradiation might result in notable changes in the necessary photophysical and photochemical properties for an effective photodynamic therapy, photostability of a prospective PS is therefore an important criterion to consider.

Table 3 summarizes the data obtained from photostability assays involving the formulations **PVP-1**, **PVP-2** and **PVP-3**. The decrease in the Soret band maximum was monitored upon irradiation with white light at an irradiance of 20 mW cm^{-2} for different irradiation periods. Under these conditions, PVP-Ps formulations were found to be photostable. **PVP-1** and **PVP-3** formulations showed a 14 % and 16 % decrease in Soret band intensity, respectively, after 30 min of irradiation, while the **PVP-2** formulation showed a 27 % decay in Soret band absorption. Despite the higher decay observed for **PVP-2** compared to **PVP-1** and **PVP-3** formulations, it can be concluded that the incorporation of porphyrin-iridium(III) complexes **1**–**3** into PVP micelles results in PVP formulations with appropriate photostability properties for use as PS in PDT.

Table 3
Photostability of PVP-PS formulations at 5 μM, after irradiation with white light at a fluence rate of 25 mW cm^{-2} for different periods of time (0–30 min).[a]

PS	λ_{max} (nm)	Irradiation time (min)									
		0	1	2	3	4	5	10	15	20	30
PVP-1	422	0	0	1	2	5	4	8	11	11	14
PVP-2	422	0	1	2	4	7	10	12	18	22	27
PVP-3	423	0	1	2	3	4	6	10	12	15	16

[a] The results are presented in percentage calculated by the ratio of residual absorbance at λ_{max} at different periods of time and absorbance before irradiation.

The capability of PVP-PS formulations to generate $^1O_2$ was evaluated by monitoring the absorption decay of 1,3-diphenylisobenzofuran (DPiBF) at 415 nm in both the absence and presence of each PVP-PS formulation. This method provides qualitative insight into the ability of a PS to generate $^1O_2$ and involves the photooxidation of the $^1O_2$ quencher, resulting in its colorless *o*-dibenzoylbenzene derivative through a Diels–Alder-like reaction [96–98]. The $^1O_2$ generation assays were performed by irradiating with red light at a fluence rate of 11 mW cm^{-2} in DMF. For comparison purposes, similar assays were performed in the presence of **PVP** without any complex and **PVP-TPP** formulations containing 5,10,15,20-tetraphenylporphyrin (TPP), recognized for its efficacy as a $^1O_2$ generator [99,100] (Fig. 3).

The results obtained from the time-dependent photodecomposition of DPiBF showed that all the considered PVP-PS formulations prepared

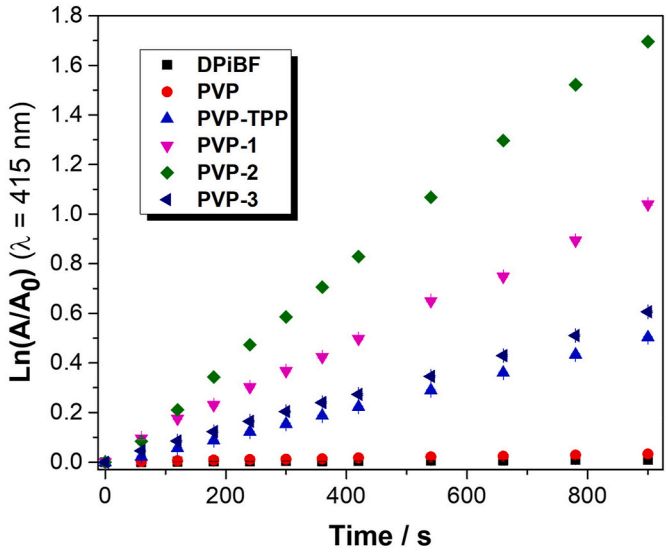

Fig. 3. Time-dependent photodecomposition of DPiBF at 50 μM in the presence of PVP-PS formulations **PVP-1**, **PVP-2**, **PVP-3** and **PVP-TPP** (PS at 0.5 μM), and of **PVP** upon irradiation with red light (630 ± 20 nm) at irradiation of 11 mW cm^{-2}. (For interpretation of the references to color in this figure legend, the reader is referred to the Web version of this article.)

are capable of generating $^1O_2$. Among them, the **PVP-2** formulation exhibited the best performance in generating the cytotoxic species, showing a 3.3-fold higher capability to generate $^1O_2$ compared to the **PVP-TPP** formulation used as a reference. Formulations **PVP-1** and **PVP-3** also displayed a good performance, inducing a decay in DPiBF absorption 2- and 1.2-fold higher, respectively, than that observed for the **PVP-TPP** formulation. It is worth noting that assays performed in the absence of PVP formulations and with the **PVP** formulation without porphyrin-based PS did not induce noticeable changes in the absorbance of DPiBF.

Overall, the characterization studies conducted for the PVP-PS formulations **PVP-1**, **PVP-2** and **PVP-3** demonstrated that the incorporation of each porphyrin bis-cyclometalated iridium(III) complex **1**–**3** is a viable strategy to overcome the low water-solubility of these derivatives, disclosing potential features for the PVP-PS formulations to be used as PS in PDT. Additionally, the prepared PVP-PS formulations retained the properties of the porphyrin-iridium(III) complexes **1**–**3** without noticeable changes, encouraging us to evaluate their effectiveness in inhibiting bladder cancer cells.

3.4. Photodynamic activity of PVP formulations against human bladder cancer cells

3.4.1. Cellular uptake of PVP formulations

The uptake of PVP-PS formulations **PVP-1**, **PVP-2** and **PVP-3** by HT-1376 cells demonstrated to be both concentration- and time dependent (Fig. 4), reaching the maximum in all cases at 12.5 μM of PS and after 4 h of incubation. **PVP-3** presented the highest intracellular accumulation in this cancer cell line (12.35 ± 5.72 nmol of PS/mg of protein) at 12.5 μM after 4 h of incubation. On the other hand, PVP formulations **PVP-1** and **PVP-2** showed similar intracellular accumulation in HT-1376 cells of 2.61 ± 0.985 and 2.86 ± 0.394 nmol of PS/mg of protein, respectively.

3.4.2. Cell viability after PDT treatment with PVP formulations

The dark toxicity and the photodynamic effect in bladder cancer cells (HT-1376 cell line) of PVP formulations **PVP-1**, **PVP-2** and **PVP-3** were evaluated at 2.5, 5.0, 10.0 and 12.5 μM. The cell line was incubated in the dark for 4 h (where it was observed higher PS intracellular accumulation) with each PVP formulation and, in the case of the photodynamic effect, cells were irradiated with white light for 40 min with an irradiance of 20 mW cm^{-2}. MTT colorimetric assay was employed to access the cell cytotoxic properties of the formulations after 24 h of treatment, either in the dark or after PDT. The results showed that **PVP-1**, **PVP-2** and **PVP-3** did not induce cytotoxicity in HT-1376 in the dark (Fig. 5A), being in accordance with one of the requirements for an ideal PS [101].

It is also possible to observe that the photodynamic effect of formulations **PVP-1**, **PVP-2** and **PVP-3** in HT-1376 cells is dependent on the aryl-substituted unit and concentration (Fig. 5B). Cytotoxic effects were significantly higher in all cases at the maximum PS concentration (12.5 μM). **PVP-2** and **PVP-3** formulations were shown to be the most efficient PS promoting a decrease up to 60 % in the cancer cell line viability. Formulation **PVP-1** did not go beyond promoting a decrease of ca. 40 % in HT-1376 cells viability. This lower PDT efficiency of **PVP-1** formulation is further supported by its higher $IC50_{PDT}$ value (25.6 μM), when compared to the $IC50_{PDT}$ values of **PVP-2** and **PVP-3** (6.97 and 7.36 μM, respectively) (Fig. 5C).

3.4.3. Cytotoxicity of PVP formulations

Envisaging the use of PVP formulations **PVP-1–3** as anticancer PS for human use, the cytotoxicity of the PVP-based formulations was determined towards Vero cells derived from the kidney of an African green monkey (*Cercopithecus aethiops)* [102]. Thus, Vero cells were exposed to **PVP-1–3** at 2.5, 5.0, 10.0 and 12.5 μM for 24 h. This was carried out according to ISO guidelines (ISO 10993-5) for *in vitro* cytotoxicity of medical devices that states that a material that promotes cell viability rates higher than 70 % compared to the control group shall be considered non-cytotoxic [74]. The results obtained are presented in Fig. 6.

The results indicated that none of the tested concentrations of the PVP formulations caused a significant reduction in the viability of the Vero cell line. According to ISO guidelines, this suggests that these formulations are considered as safe for clinical use.

The last years have been highly significant in the search for new PS that preferentially accumulates within the target tumor tissue. Conjugation with active targets [84], the use of peptides and antibodies [103, 104], and encapsulation in drug-delivery systems that could deliver the

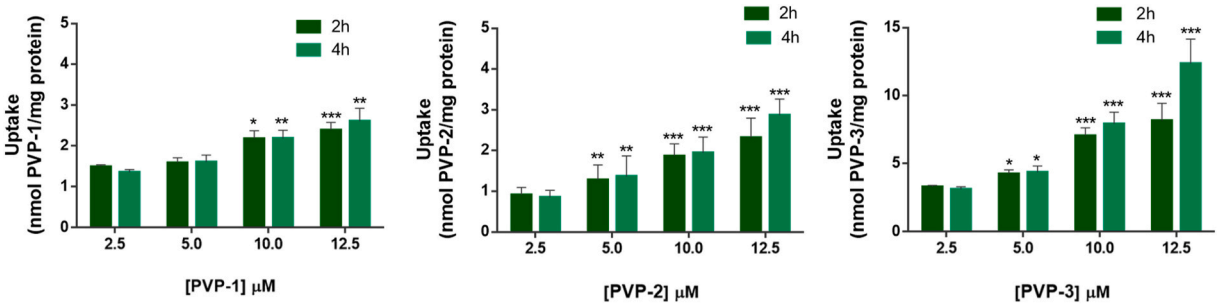

Fig. 4. Intracellular uptake of formulations **PVP-1, PVP-2 and PVP-3** by HT-1376 cells. Data are the mean ± S.D. of at least three independent experiments performed in triplicates: *($p < 0.05$), **($p < 0.01$), ***($p < 0.001$) significantly different from uptake of PVP formulations at 2.5 μM.

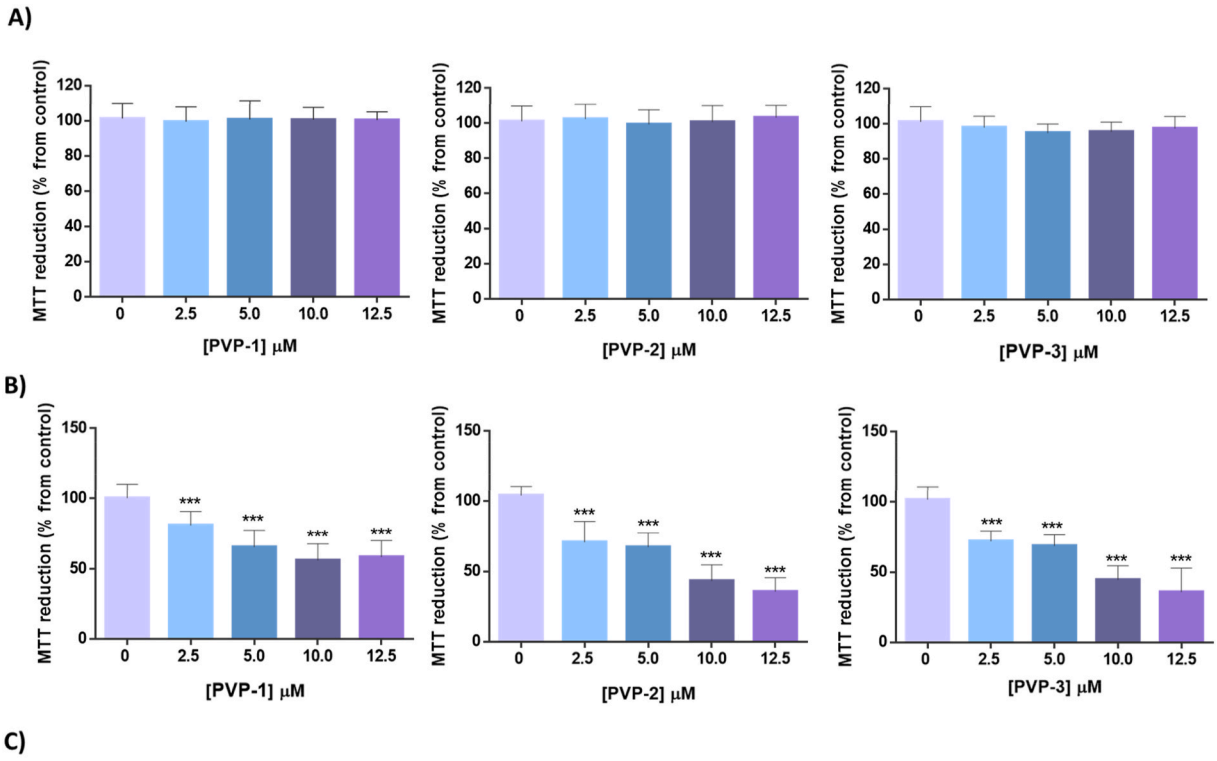

PVP Formulation	$IC50_{PDT}$ *
PVP-1	25.6 μM
PVP-2	6.97 μM
PVP-3	7.36 μM

* Calculated by extrapolation from the non-linear regression curve MTT reduction (% from control) vs. log(concentration).

Fig. 5. Cytotoxicity of formulations **PVP-1**, **PVP-2** and **PVP-3** in HT-1376 bladder cancer cells. A) HT-1376 cells were incubated in the dark for 4 h with each formulation **PVP-1**, **PVP-2** and **PVP-3** and cytotoxicity was evaluated 24 h after treatment using the MTT assay. The percentage of cytotoxicity was expressed relatively to control cells (cells incubated with PBS) **(B)** Phototoxic effects of **PVP-1, PVP-2 and PVP-3** in HT-1376 cells 24 h after PDT (irradiation with white light for 40 min; fluence rate of 20 mW cm^{-2}). The percentage of cytotoxicity was expressed relative to control cells (cells incubated with PBS and irradiated). Data are the mean value ± S.D. of at least three independent experiments performed in triplicates: *($p < 0.05$), **($p < 0.01$), ***($p < 0.001$) compared to MTT reduction (%) at 24 h after PDT for control cells (untreated cells). (**C**) $IC50_{PDT}$ (μM) values of **PVP-1**, **PVP-2** and **PVP-3** formulations in HT-1376 cell line (for a fluence rate of 20 mW cm^{-2}).

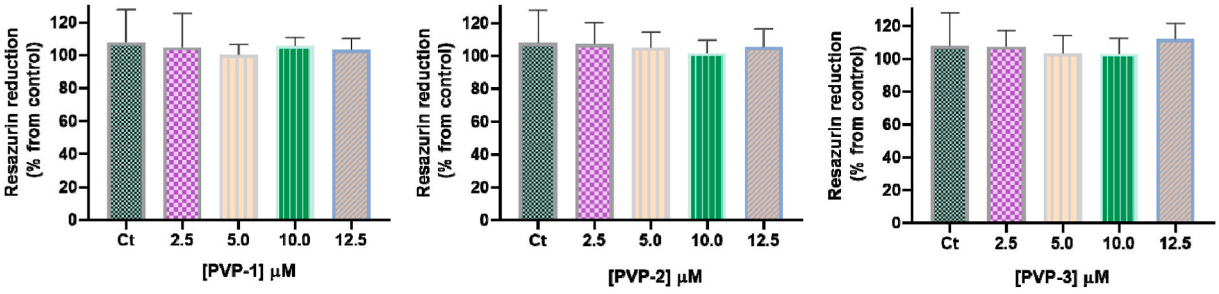

Fig. 6. Cytotoxicity of formulations **PVP-1**, **PVP-2** and **PVP-3** in Vero Cells. These were incubated in the dark for 24 h with formulations **PVP-1**, **PVP-2** and **PVP-3** and cytotoxicity was evaluated after this period using the resazurin assay. The percentage of cytotoxicity was expressed relatively to control cells (Ct).

PS into tumor cells [105], are some of the strategies adopted to reach that goal.

It is widely recognized that PVP polymer forms pH-sensitive polymeric micelles for extracellular and intracellular drug release, with its internalization being mediated by endocytosis [106]. Thus, PVP particles have the capacity to release drugs in response to the acidic extracellular fluids of tumor tissue. This fact suggests that interstitial pH in tumor tissue is important for PS liberation. The higher accumulation, and therefore the remarkable photodynamic effect of **PVP-1, PVP-2** and **PVP-3** formulations in HT-1376 cells, could be attributed to the tumor

surface adhesion [107] and/or efficient release of the formulation PS content into the cytoplasm, mediated by the pH variations [84].

However, the efficiency of PDT is not solely determined by PS uptake in cancer. Generation of $^1O_2$ and other ROS, aggregation, and photodegradation behavior are other properties that must be considered [10]. PVP formulations **PVP-1, PVP-2** and **PVP-3** demonstrate to be photostable under the studied irradiation conditions, although showing different $^1O_2$ generation profiles. The **PVP-2** formulation demonstrated the highest efficiency in generating $^1O_2$ and despite not having the highest accumulation in cancer cells, it induced the higher rates in the decrease of cells viability and had the lower $IC50_{PDT}$ value. On the other hand, **PVP-3** exhibited a lower $^1O_2$ generation profile compared to its analogues **PVP-1** and **PVP-2**. However, its remarkable accumulation in HT-1376 cells enhanced its PDT effect, resulting in an $IC50_{PDT}$ value and a cell viability decrease rate similar to that of **PVP-2**. Since PVP does not negatively affect the viability of HT-1376 cells, as previously reported [84], the observed effects can be attributed solely to the action of the photosensitizers.

Another crucial aspect to consider is the safety of **PVP-1–3** formulations for human use. PVP formulations have already been shown to be biocompatible, non-toxic, and highly effective in drug delivery systems [79]. In this study, the PVP formulations showed to be non-cytotoxic for a normal cell line, since no reduction in the viability of Vero cells was observed. This highlights the potential for these formulations to be safely used in the PDT treatment of bladder cancer. This safety could be also reinforced by favorable pharmacokinetics, good stability in biological environments, excellent uptake, faster clearance rates and reduced off-target effects of iridium-based complexes compared to traditional porphyrins, which enhances their therapeutic potential [108,109]. Some studies highlight the ability of these complexes to target mitochondria and lysosomes, providing selective action and minimizing systemic effect [109,110].

The use of these formulations in the PDT treatment of bladder cancer offers enormous advantages in such localized treatment, if the PS and the irradiation were applied locally, offering a promising alternative or adjunct to traditional therapies such as surgery, chemotherapy, and radiotherapy [111]. Its ability to provide targeted, minimally invasive, and repeatable treatment with minimal systemic toxicity makes it a promising option for patients who may not tolerate aggressive therapies [112,113].

4. Conclusions

In summary, porphyrin bis-cyclometalated iridium(III) complexes were successfully incorporated into PVP micelles affording PVP-PS formulations. This strategy allowed the preservation of the photophysical and photochemical properties of the porphyrin-based PS while enhancing water-solubility features. Moreover, the PVP-PS formulations exhibited stability under the evaluated light irradiation conditions and also demonstrated remarkable $^1O_2$ generation performances. These properties suggest that such species can be considered as useful candidates to be used as PS in PDT.

PVP formulations demonstrated higher cellular uptake by HT-1376 cells, with particular emphasis on **PVP-3**, with a remarkable internalization rate. This formulation and **PVP-2** were the most efficient PS, promoting a decrease in HT-1376 cell viability higher than 60 %, demonstrating the lower $IC50_{PDT}$ values. Moreover, the tested formulations did not show dark toxicity towards the HT-1376 cell line, attesting the dependency of ROS production under irradiation for the photodynamic effect. This study also demonstrates that PVP-based formulations could offer a safe and effective approach for PDT in bladder cancer since no cytotoxic effects were observed in Vero cells, providing a localized, minimally invasive treatment option with minimal systemic toxicity, potentially complementing or replacing more aggressive therapies.

These promising results could boost new strategies for the synthesis and *in vitro* and *in vivo* evaluation of PVP formulation based on porphyrinic bis-cyclometalated iridium(III) complexes as new PDT agents.

CRediT authorship contribution statement

Nuno M.M. Moura: Writing – review & editing, Writing – original draft, Methodology, Investigation, Conceptualization. **Melani J.A. Reis:** Investigation. **Carlos Lodeiro:** Writing – review & editing, Validation. **M. Graça P.M. S. Neves:** Writing – review & editing, Validation, Formal analysis. **José A.S. Cavaleiro:** Writing – review & editing, Validation. **Carlos F. Ribeiro:** Writing – review & editing, Validation. **Rosa Fernandes:** Writing – review & editing, Validation, Formal analysis. **Ana T. P.C. Gomes:** Writing – review & editing, Writing – original draft, Supervision, Methodology, Investigation, Conceptualization.

Funding

This research work received financial support from the University of Aveiro and Fundação para a Ciência e Tecnologia and Ministério da Ciência, Tecnologia e Ensino Superior (FCT/MCTES) to support the LAQV-REQUIMTE (LA/P/0008/2020 DOI 10.54499/LA/P/0008/2020, UIDP/50006/2020 DOI 10.54499/UIDP/50006/2020 and UIDB/50006/2020 DOI 10.54499/UIDB/50006/2020) research unit through national funds and, where applicable, was co-financed by the FEDER, within the PT2020 Partnership Agreement, and to the Portuguese NMR Network. NMM Moura and ATPC Gomes thanks FCT for funding through program DL 57/2016 – Norma transitória (CDL-CTTRI-048-88-ARH/2018) and (CEECINST/00137/2018/CP1520/CT0022), respectively. MJA Reis thanks FCT for her PhD grant (2020.05838.BD).

Declaration of competing interest

The authors declare that they have no known competing financial interests or personal relationships that could have appeared to influence the work reported in this paper.

Acknowledgments

The authors thank the University of Aveiro and FCT/MCTES for financial support to LAQV-REQUIMTE (LA/P/0008/2020, and UIDP/50006/2020 and UIDB/50006/2020) research units, and Portuguese NMR Network. "The NMR spectrometers are part of the National NMR Network (PTNMR) and are partially supported by Infrastructure Project Nº 022161 (co-financed by FEDER through COMPETE 2020, POCI and PORL and FCT through PIDDAC).

Appendix A. Supplementary data

Supplementary data to this article can be found online at https://doi.org/10.1016/j.dyepig.2024.112580.

Data availability

Data will be made available on request.

References

[1] Kar B, Das U, Roy N, Paira P. Recent advances on organelle specific Ru(II)/Ir(III)/Re(I) based complexes for photodynamic therapy. Coord Chem Rev 2023;474:214860. https://doi.org/10.1016/J.CCR.2022.214860.

[2] Sung H, Ferlay J, Siegel RL, Laversanne M, Soerjomataram I, Jemal A, et al. Global cancer statistics 2020: GLOBOCAN estimates of incidence and mortality worldwide for 36 cancers in 185 countries. CA A Cancer J Clin 2021;71:209–49. https://doi.org/10.3322/caac.21660.

[3] Liu H, Lu C, Han L, Zhang X, Song G. Optical – magnetic probe for evaluating cancer therapy. Coord Chem Rev 2021;441:213978. https://doi.org/10.1016/j.ccr.2021.213978.

[4] Su S, Chen Y, Zhang P, Ma R, Zhang W, Liu J, et al. The role of Platinum(IV)-based antitumor drugs and the anticancer immune response in medicinal inorganic chemistry. A systematic review from 2017 to 2022. Eur J Med Chem 2022;243:114680. https://doi.org/10.1016/J.EJMECH.2022.114680.

[5] Yu C, Wang Z, Sun Z, Zhang L, Zhang W, Xu Y, et al. Platinum-based combination therapy: molecular rationale, current clinical uses, and future perspectives. J Med Chem 2020;63:13397–412. https://doi.org/10.1021/acs.jmedchem.0c00950.

[6] Hang Z, Cooper MA, Ziora ZM. Platinum-based anticancer drugs encapsulated liposome and polymeric micelle formulation in clinical trials. Biochem Comp 2016;4:1. https://doi.org/10.7243/2052-9341-4-2.

[7] Facchetti G, Rimoldi I. Anticancer platinum(II) complexes bearing N-heterocycle rings. Bioorg Med Chem Lett 2019;29:1257–63. https://doi.org/10.1016/j.bmcl.2019.03.045.

[8] Cocetta V, Ragazzi E, Montopoli M. Mitochondrial involvement in cisplatin resistance. Int J Mol Sci 2019;20:3384. https://doi.org/10.3390/ijms20143384.

[9] Martinho N, Santos TCB, Florindo HF, Silva LC. Cisplatin-membrane interactions and their influence on platinum complexes activity and toxicity. Front Physiol 2019;9:1898. https://doi.org/10.3389/fphys.2018.01898.

[10] Gomes ATPC, Neves MGPMS, Fernandes R, Ribeiro CF, Cavaleiro JAS, Moura NMM. Unraveling the photodynamic activity of cationic benzoporphyrin-based photosensitizers against bladder cancer cells. Molecules 2021;26:5312. https://doi.org/10.3390/molecules26175312.

[11] Aoki S, Yokoi K, Hisamatsu Y, Balachandran C, Tamura Y, Tanaka T. Post-complexation functionalization of cyclometalated iridium(III) complexes and applications to biomedical and material sciences. Top Curr Chem 2022;380:1–43. https://doi.org/10.1007/S41061-022-00401-W. 3805 2022.

[12] Shi H, Wang Y, Lin S, Lou J, Zhang Q. Recent development and application of cyclometalated iridium(III) complexes as chemical and biological probes. Dalton Trans 2021;50:6410–7. https://doi.org/10.1039/D1DT00592H.

[13] Rota Martir D, Zysman-Colman E. Supramolecular iridium(III) assemblies. Coord Chem Rev 2018;364:86–117. https://doi.org/10.1016/J.CCR.2018.03.016.

[14] Ito A, Iwamura M, Sakuda E. Excited-state dynamics of luminescent transition metal complexes with metallophilic and donor–acceptor interactions. Coord Chem Rev 2022;467:214610. https://doi.org/10.1016/J.CCR.2022.214610.

[15] Zhang Y, Qiao J. Near-infrared emitting iridium complexes: molecular design, photophysical properties, and related applications. iScience 2021;24:102858. https://doi.org/10.1016/J.ISCI.2021.102858.

[16] Chen QF, Guo YH, Yu YH, Zhang MT. Bioinspired molecular clusters for water oxidation. Coord Chem Rev 2021;448:214164. https://doi.org/10.1016/J.CCR.2021.214164.

[17] Yoon S, Teets TS. Red to near-infrared phosphorescent Ir(III) complexes with electron-rich chelating ligands. Chem Commun 2021;57:1975–88. https://doi.org/10.1039/D0CC08067E.

[18] Woźniak Ł, Tan JF, Nguyen QH, Madron Du Vigné A, Smal V, Cao YX, et al. Catalytic enantioselective functionalizations of C–H bonds by chiral iridium complexes. Chem Rev 2020;120:10516–43. https://doi.org/10.1021/ACS.CHEMREV.0C00559.

[19] Colombo A, Dragonetti C, Guerchais V, Hierlinger C, Zysman-Colman E, Roberto DA. Trip in the nonlinear optical properties of iridium complexes. Coord Chem Rev 2020;414:213293. https://doi.org/10.1016/J.CCR.2020.213293.

[20] Hong G, Gan X, Leonhardt C, Zhang Z, Seibert J, Busch JM, et al. A brief history of OLEDs—emitter development and industry milestones. Adv Mater 2021;33:2005630. https://doi.org/10.1002/ADMA.202005630.

[21] Schwehr BJ, Hartnell D, Massi M, Hackett MJ, Kam-Wing Lo K, Kam-Keung Leung P, et al. Luminescent metal complexes as emerging tools for lipid imaging. Top Curr Chem 2022 3806 2022;380:1–40. https://doi.org/10.1007/S41061-022-00400-X.

[22] Jhun BH, Song D, Park SY, You Y. Phosphorescent Ir(III) complexes for biolabeling and biosensing. Top Curr Chem 2022;380:1–40. https://doi.org/10.1007/S41061-022-00389-3. 3805 2022.

[23] Tyagi K, Dixit T, Venkatesh V. Recent advances in catalytic anticancer drugs: mechanistic investigations and future prospects. Inorg Chim Acta 2022;533:120754. https://doi.org/10.1016/J.ICA.2021.120754.

[24] Sharma SA, P S, Roy N, Paira P. Advances in novel iridium (III) based complexes for anticancer applications: a review. Inorg Chim Acta 2020;513:119925. https://doi.org/10.1016/J.ICA.2020.119925.

[25] Lu L, Liu LJ, Chao WC, Zhong HJ, Wang M, Chen XP, et al. Identification of an iridium(III) complex with anti-bacterial and anti-cancer activity. Sci Rep 2015 51 2015;5:14544. https://doi.org/10.1038/srep14544.

[26] Gourdon L, Cariou K, Gasser G. Phototherapeutic anticancer strategies with first-row transition metal complexes: a critical review. Chem Soc Rev 2022;51:1167–95. https://doi.org/10.1039/D1CS00609F.

[27] Li J, Chen T. Transition metal complexes as photosensitizers for integrated cancer theranostic applications. Coord Chem Rev 2020;418:213355. https://doi.org/10.1016/j.ccr.2020.213355.

[28] Huang L, Zhao S, Wu J, Yu L, Singh N, Yang K, et al. Photodynamic therapy for hypoxic tumors: advances and perspectives. Coord Chem Rev 2021;438:213888. https://doi.org/10.1016/j.ccr.2021.213888.

[29] Chen D, Xu Q, Wang W, Shao J, Huang W, Dong X. Type I photosensitizers revitalizing photodynamic oncotherapy. Small 2021:2006742. https://doi.org/10.1002/smll.202006742.

[30] Yang B, Chen Y, Shi J. Reactive oxygen species (ROS)-Based nanomedicine. Chem Rev 2019;119:4881–985. https://doi.org/10.1021/acs.chemrev.8b00626.

[31] Gomes ATPC, Neves MGPMS, Cavaleiro JAS. Cancer, photodynamic therapy and porphyrin-type derivatives. An Acad Bras Cienc 2018;90:993–1026. https://doi.org/10.1590/0001-3765201820170811.

[32] Dąbrowski JM, Pucelik B, Regiel-Futyra A, Brindell M, Mazuryk O, Kyzioł A, et al. Engineering of relevant photodynamic processes through structural modifications of metallotetrapyrrolic photosensitizers. Coord Chem Rev 2016;325:67–101. https://doi.org/10.1016/j.ccr.2016.06.007.

[33] Kwon N, Kim H, Li X, Yoon J. Supramolecular agents for combination of photodynamic therapy and other treatments. Chem Sci 2021;12:7248–68. https://doi.org/10.1039/d1sc01125a.

[34] Sandland J, Malatesti N, Boyle R. Porphyrins and related macrocycles: combining photosensitization with radio- or optical-imaging for next generation theranostic agents. Photodiagnosis Photodyn Ther 2018;23:281–94. https://doi.org/10.1016/j.pdpdt.2018.06.023.

[35] Zhang Q, He J, Yu W, Li Y, Liu Z, Zhou B, et al. A promising anticancer drug: a photosensitizer based on the porphyrin skeleton. RSC Med Chem 2020;11:427–37. https://doi.org/10.1039/c9md00558g.

[36] Mesquita MQ, Dias CJ, Neves MGPMS, Almeida A, Faustino MAF. Revisiting current photoactive materials for antimicrobial photodynamic therapy. Molecules 2018;23:2424. https://doi.org/10.3390/molecules23102424.

[37] Vieira C, Gomes ATPC, Mesquita MQ, Moura NMM, Neves MGPMS, Faustino MAF, et al. An insight into the potentiation effect of potassium iodide on aPDT efficacy. Front Microbiol 2018;9:2665. https://doi.org/10.3389/fmicb.2018.02665.

[38] Kadish KM, Smith KM, Guilard R. Handbook of porphyrin science. Singapore: World Scientific Publishing Company; 2010.

[39] Lee H, Hong KI, Jang WD. Design and applications of molecular probes containing porphyrin derivatives. Coord Chem Rev 2018;354:46–73. https://doi.org/10.1016/j.ccr.2017.06.008.

[40] Paolesse R, Nardis S, Monti D, Stefanelli M, Di Natale C. Porphyrinoids for chemical sensor applications. Chem Rev 2017;117:2517–83. https://doi.org/10.1021/acs.chemrev.6b00361.

[41] Moura NMM, Núñez C, Santos SM, Faustino MAF, Cavaleiro JAS, Neves MGPMS, et al. Synthesis, spectroscopy studies, and theoretical calculations of new fluorescent probes based on pyrazole containing porphyrins for Zn(II), Cd(II), and Hg(II) optical detection. Inorg Chem 2014;53:6149–58. https://doi.org/10.1021/ic500634y.

[42] Chen YZ, Jiang DJ, Gong ZQ, Li QL, Shi RR, Yang ZX, et al. Visible-light responsive organic nano-heterostructured photocatalysts for environmental remediation and H-2 generation. J Mater Sci Technol 2020;38:93–106. https://doi.org/10.1016/j.jmst.2019.09.003.

[43] Radi S, El Abiad C, Moura NMM, Faustino MAF, Neves MGPMS. New hybrid adsorbent based on porphyrin functionalized silica for heavy metals removal: synthesis, characterization, isotherms, kinetics and thermodynamics studies. J Hazard Mater 2019;370:80–90. https://doi.org/10.1016/j.jhazmat.2017.10.058.

[44] Abiad CE, Radi S, Faustino MAF, Graça Neves MPMS, Moura NMM. Supramolecular hybrid material based on engineering porphyrin hosts for an efficient elimination of lead(II) from aquatic medium. Molecules 2019;24:669. https://doi.org/10.3390/molecules24040669.

[45] Neves CMB, Filipe OMS, Mota N, Santos SAO, Silvestre AJD, Santos EBH, et al. Photodegradation of metoprolol using a porphyrin as photosensitizer under homogeneous and heterogeneous conditions. J Hazard Mater 2019;370:13–23. https://doi.org/10.1016/j.jhazmat.2018.11.055.

[46] Pegis ML, Wise CF, Martin DJ, Mayer JM. Oxygen reduction by homogeneous molecular catalysts and electrocatalysts. Chem Rev 2018;118:2340–91. https://doi.org/10.1021/acs.chemrev.7b00542.

[47] Da Silva ES, Moura NMM, Neves MGPMS, Coutinho A, Prieto M, Silva CG, et al. Novel hybrids of graphitic carbon nitride sensitized with free-base meso-tetrakis (carboxyphenyl) porphyrins for efficient visible light photocatalytic hydrogen production. Appl Catal B Environ 2018;221:56–69. https://doi.org/10.1016/j.apcatb.2017.08.079.

[48] Zhang W, Lai W, Cao R. Energy-related small molecule activation reactions: oxygen reduction and hydrogen and oxygen evolution reactions catalyzed by porphyrin- and corrole-based systems. Chem Rev 2017;117:3717–97. https://doi.org/10.1021/acs.chemrev.6b00299.

[49] Costentin C, Robert M, Savéant JM. Current issues in molecular catalysis illustrated by iron porphyrins as catalysts of the CO2-to-CO electrochemical conversion. Acc Chem Res 2015;48:2996–3006. https://doi.org/10.1021/acs.accounts.5b00262.

[50] Asselin P, Harvey PD. Visible-light-Driven production of solar fuels catalyzed by nanosized porphyrin-based metal–organic frameworks and covalent–organic frameworks: a review. ACS Appl Nano Mater 2022;5:6055–82. https://doi.org/10.1021/acsanm.2c00831.

[51] Sekaran B, Misra R. β-Pyrrole functionalized porphyrins: synthesis, electronic properties, and applications in sensing and DSSC. Coord Chem Rev 2022;453:214312. https://doi.org/10.1016/J.CCR.2021.214312.

[52] Gopalakrishnan VN, Becerra J, Pena EF, Sakar M, Béland F, Do TO. Porphyrin and single atom featured reticular materials: recent advances and future perspective of solar-driven CO2 reduction. Green Chem 2021;23:8332–60. https://doi.org/10.1039/D1GC02439F.

[53] Park JM, Hong K-I, Lee H, Jang W-D. Bioinspired applications of porphyrin derivatives. Acc Chem Res 2021;54:2249–60. https://doi.org/10.1021/acs.accounts.1c00114.

[54] Di Carlo G, Biroli AO, Tessore F, Caramori S, Pizzotti M. beta-Substituted Zn-II porphyrins as dyes for DSSC: a possible approach to photovoltaic windows. Coord Chem Rev 2018;358:153–77. https://doi.org/10.1016/j.ccr.2017.12.012.

[55] Li Y, Chen Q, Pan X, Lu W, Zhang J. New insight into the application of fluorescence platforms in tumor diagnosis: from chemical basis to clinical application. Med Res Rev 2022:1–44. https://doi.org/10.1002/MED.21932.

[56] Chan WL, Xie C, Lo WS, Bünzli JCG, Wong WK, Wong KL. Lanthanide–tetrapyrrole complexes: synthesis, redox chemistry, photophysical properties, and photonic applications. Chem Soc Rev 2021;50:12189–257. https://doi.org/10.1039/C9CS00828D.

[57] Castro KADF, Ramos L, Mesquita M, Biazzotto JC, Moura NMM, Mendes RF, et al. Comparison of the photodynamic action of porphyrin, chlorin, and isobacteriochlorin derivatives toward a melanotic cell line. ACS Appl Bio Mater 2021;4:4925–35. https://doi.org/10.1021/acsabm.1c00218.

[58] Almeida-Marrero V, Gonzalez-Delgado JA, Torres T. Emerging perspectives on applications of porphyrinoids for photodynamic therapy and photoinactivation of microorganisms. Macroheterocycles 2019;12:8–16. https://doi.org/10.6060/mhc181220t.

[59] McKenzie LK, Bryant HE, Weinstein JA. Transition metal complexes as photosensitisers in one- and two-photon photodynamic therapy. Coord Chem Rev 2019;379:2–29. https://doi.org/10.1016/j.ccr.2018.03.020.

[60] Moura NMM, Monteiro CJP, Tomé AC, Neves MGPMS, Cavaleiro JAS. Synthesis of chlorins and bacteriochlorins from cycloaddition reactions with porphyrins. ARKIVOC (Gainesville, FL, U S) 2022:54–98. https://doi.org/10.24820/ark.5550190.p011.696.

[61] Gamelas SRD, Moura NMM, Habraken Y, Piette J, Neves MGPMS, Faustino MAF. Tetracationic porphyrin derivatives against human breast cancer. J Photochem Photobiol B Biol 2021;222:112258. https://doi.org/10.1016/j.jphotobiol.2021.112258.

[62] Eddahmi M, Sousa V, Moura NMM, Dias CJ, Bouissane L, Faustino MAF, et al. New nitroindazole-porphyrin conjugates: synthesis, characterization and antibacterial properties. Bioorg Chem 2020;101:103994. https://doi.org/10.1016/j.bioorg.2020.103994.

[63] Hamblin MR. Antimicrobial photodynamic inactivation: a bright new technique to kill resistant microbes. Curr Opin Microbiol 2016;33:67–73. https://doi.org/10.1016/j.mib.2016.06.008.

[64] Fathi P, Pan Di. Current trends in pyrrole and porphyrin-derived nanoscale materials for biomedical applications, vol. 15; 2020. p. 2493–515. https://doi.org/10.2217/NNM-2020-0125.

[65] Menilli L, Monteiro AR, Lazzarotto S, Morais FMP, Gomes ATPC, Moura NMM, et al. Graphene oxide and graphene quantum dots as delivery systems of cationic porphyrins: photo-antiproliferative activity evaluation towards t24 human bladder cancer cells. Pharmaceutics 2021;13:1512. https://doi.org/10.3390/PHARMACEUTICS13091512/S1.

[66] Vallejo MCS, Reis MJA, Pereira AMVM, Serra VV, Cavaleiro JAS, Moura NMM, et al. Merging pyridine(s) with porphyrins and analogues: an overview of synthetic approaches. Dyes Pigments 2021;191:109298. https://doi.org/10.1016/j.dyepig.2021.109298.

[67] Pham TC, Nguyen V-N, Choi Y, Lee S, Yoon J. Recent strategies to develop innovative photosensitizers for enhanced photodynamic therapy. Chem Rev 2021;121:13454–619. https://doi.org/10.1021/acs.chemrev.1c00381.

[68] Zhang L, Geng Y, Li L, Tong X, Liu S, Liu X, et al. Rational design of iridium–porphyrin conjugates for novel synergistic photodynamic and photothermal therapy anticancer agents. Chem Sci 2021;12:5918–25. https://doi.org/10.1039/D1SC00126D.

[69] Moura NMM, Cuerva C, Cavaleiro JAS, Mendes RF, Paz FAA, Cano M, et al. Metallomesogens with luminescent behaviour: palladium complexes derived from alkylamide tetraarylporphyrins. Chempluschem 2016;81:262–73. https://doi.org/10.1002/cplu.201500557.

[70] Moura NMM, Castro KADF, Biazzotto JC, Prandini JA, Lodeiro C, Faustino MAF, et al. Ruthenium and iridium complexes bearing porphyrin moieties: PDT efficacy against resistant melanoma cells. Dyes Pigments 2022;205:110501. https://doi.org/10.1016/J.DYEPIG.2022.110501.

[71] Ermilov EA, Büge B, Jasinski S, Jux N, Röder B. Spectroscopic study of NH-tautomerism in novel cycloketo-tetraphenylporphyrins. J Chem Phys 2009;130:134509. https://doi.org/10.1063/1.3098316.

[72] Moura NMM, Serra VV, Bastos A, Biazotto JC, Castro KADF, Faustino MAF, et al. New bis-cyclometalated iridium(III) complexes with β-substituted porphyrin-arylbipyridine as the ancillary ligand: electrochemical and photophysical insights. Int J Mol Sci 2022;23:7606. https://doi.org/10.3390/ijms23147606.

[73] Bhaumik J, Weissleder R, McCarthy JR. Synthesis and photophysical properties of sulfonamidophenyl porphyrins as models for activatable photosensitizers. J Org Chem 2009;74:5894–901. https://doi.org/10.1021/jo900832y.

[74] ISO. ISO10993-5. In: Biol. Eval. Med. Devices — Part 5 tests vitr. Geneva, Switzerland: Cytotox.; 2009.

[75] Mehring A, Erdmann N, Walther J, Stiefelmaier J, Strieth D, Ulber R. A simple and low-cost resazurin assay for vitality assessment across species. J Biotechnol 2021;333:63–6. https://doi.org/10.1016/j.jbiotec.2021.04.010.

[76] The n-octanol:water partition coefficients (miLog P) were evaluated using the MolinspirationWebME Editor 3.81, http://www.molinspiration.com (accessed august 2021). n.d.

[77] Kurakula M, Rao GSNK. Pharmaceutical assessment of polyvinylpyrrolidone (PVP): as excipient from conventional to controlled delivery systems with a spotlight on COVID-19 inhibition. J Drug Deliv Sci Technol 2020;60:102046. https://doi.org/10.1016/J.JDDST.2020.102046.

[78] Luo Y, Hong Y, Shen L, Wu F, Lin X. Multifunctional role of polyvinylpyrrolidone in pharmaceutical formulations. AAPS PharmSciTech 2021;22:34. https://doi.org/10.1208/S12249-020-01909-4.

[79] Franco P, De Marco I. The use of poly(N-vinyl pyrrolidone) in the delivery of drugs: a review. Polymers 2020;12:1114. https://doi.org/10.3390/POLYM12051114.

[80] Isakau HA, Parkhats MV, Knyukshto VN, Dzhagarov BM, Petrov EP, Petrov PT. Toward understanding the high PDT efficacy of chlorin e6-polyvinylpyrrolidone formulations: Photophysical and molecular aspects of photosensitizer-polymer interaction in vitro. J Photochem Photobiol B Biol 2008;92:165–74. https://doi.org/10.1016/j.jphotobiol.2008.06.004.

[81] Kashef N, Huang Y-YY, Hamblin MR. Advances in antimicrobial photodynamic inactivation at the nanoscale, vol. 6. Walter de Gruyter GmbH; 2017. https://doi.org/10.1515/nanoph-2016-0189.

[82] Schwach-Abdellaoui K, Vivien-Castioni N, Gurny R. Local delivery of antimicrobial agents for the treatment of periodontal diseases. Eur J Pharm Biopharm 2000;50:83–99. https://doi.org/10.1016/S0939-6411(00)00086-2.

[83] Cardoso M, Gomes ATPC, Moreira C, Simões MMQ, Neves MGPMS, da Rocha D, et al. Efficient catalytic oxidation of 3-arylthio- and 3-Cyclohexylthio-lapachone derivatives to new sulfonyl derivatives and evaluation of their antibacterial activities. Molecules 2017;22:302. https://doi.org/10.3390/molecules22020302.

[84] Gomes ATPC, Fernandes R, Ribeiro CF, Tomé JPC, Neves MGPMS, da Silva F de C, et al. Synthesis, characterization and photodynamic activity against bladder cancer cells of novel triazole-porphyrin derivatives. Molecules 2020;25:1607. https://doi.org/10.3390/molecules25071607.

[85] Danaei M, Dehghankhold M, Ataei S, Hasanzadeh Davarani F, Javanmard R, Dokhani A, et al. Impact of particle size and polydispersity index on the clinical applications of lipidic nanocarrier systems. Pharmaceutics 2018;10:57. https://doi.org/10.3390/pharmaceutics10020057.

[86] Liberti MV, Locasale JW. The warburg effect: how does it benefit cancer cells? Trends Biochem Sci 2016;41:211–8. https://doi.org/10.1016/j.tibs.2015.12.001.

[87] Ernsting MJ, Murakami M, Roy A, Li S-D. Factors controlling the pharmacokinetics, biodistribution and intratumoral penetration of nanoparticles. J Contr Release 2013;172:782–94. https://doi.org/10.1016/j.jconrel.2013.09.013.

[88] Lu Y, Park K. Polymeric micelles and alternative nanonized delivery vehicles for poorly soluble drugs. Int J Pharm 2013;453:198–214. https://doi.org/10.1016/j.ijpharm.2012.08.042.

[89] Hashimoto T, Choe YK, Nakano H, Hirao K. Theoretical study of the Q and B bands of free-base, magnesium, and zinc porphyrins, and their derivatives. J Phys Chem A 1999;103:1894–904. https://doi.org/10.1021/jp984807d.

[90] Maximiano RV, Piovesan E, Zílio SC, Machado AEH, De Paula R, Cavaleiro JAS, et al. Excited-state absorption investigation of a cationic porphyrin derivative. J Photochem Photobiol Chem 2010;214:115–20. https://doi.org/10.1016/j.jphotochem.2010.06.007.

[91] Baskin JS, Yu HZ, Zewail AH. Ultrafast dynamics of porphyrins in the condensed phase: I. Free base tetraphenylporphyrin. J Phys Chem A 2002;106:9837–44. https://doi.org/10.1021/jp020398g.

[92] Ohno O, Kaizu Y, Kobayashi H. Luminescence of some metalloporphins including the complexes of the IIIb metal group. J Chem Phys 1985;82:1779–87. https://doi.org/10.1063/1.448410.

[93] Seybold PG, Gouterman M. Porphyrins. XIII: fluorescence spectra and quantum yields. J Mol Spectrosc 1969;31:1–13. https://doi.org/10.1016/0022-2852(69)90335-X.

[94] Montalti M, Credi A, Prodi L, Gandolfi MT. Handbook of photochemistry. third ed. Boca Raton, USA: Taylor and Francis Inc; 2006.

[95] Berlman IB. Handbook of fluorescence spectra of aromatic molecules. second ed. New York, USA: Academic Press; 1971.

[96] Zimcik P, Miletin M, Radilova H, Novakova V, Kopecky K, Svec J, et al. Synthesis, properties and *in vitro* photodynamic activity of water-soluble azaphthalocyanines and azanaphthalocyanines. Photochem Photobiol 2010;86:168–75. https://doi.org/10.1111/j.1751-1097.2009.00647.x.

[97] Spesia MB, Milanesio ME, Durantini EN. Synthesis, properties and photodynamic inactivation of *Escherichia coli* by novel cationic fullerene C60 derivatives. Eur J Med Chem 2008;43:853–61. https://doi.org/10.1016/j.ejmech.2007.06.014.

[98] Spiller W, Kliesch H, Wöhrle D, Hackbarth S, Röder B, Schnurpfeil G. Singlet oxygen quantum yields of different photosensitizers in polar solvents and micellar solutions. J Porphyr Phthalocyanines 1998;2:145–58. https://doi.org/10.1002/(SICI)1099-1409(199803/04)2:2<145::AID-JPP60>3.0.CO;2-158.

[99] Moura NMM, Faustino MAF, Neves MGPMS, Tomé AC, Rakib EM, Hannioui A, et al. Novel pyrazoline and pyrazole porphyrin derivatives: synthesis and photophysical properties. Tetrahedron 2012;68:8181–93. https://doi.org/10.1016/j.tet.2012.07.072.

[100] Zenkevich E, Sagun E, Knyukshto V, Shulga A, Mironov A, Efremova O, et al. Photophysical and photochemical properties of potential porphyrin and chlorin photosensitizers for PDT. J Photochem Photobiol B Biol 1996;33:171–80. https://doi.org/10.1016/1011-1344(95)07241-1.

[101] Ostańska E, Aebisher D, Bartusik-Aebisher D. The potential of photodynamic therapy in current breast cancer treatment methodologies. Biomed Pharmacother 2021;137:111302. https://doi.org/10.1016/J.BIOPHA.2021.111302.

[102] Kiesslich S, Kamen AA. Vero cell upstream bioprocess development for the production of viral vectors and vaccines. Biotechnol Adv 2020;44:107608. https://doi.org/10.1016/j.biotechadv.2020.107608.

[103] Mitsunaga M, Ogawa M, Kosaka N, Rosenblum LT, Choyke PL, Kobayashi H. Cancer cell–selective in vivo near infrared photoimmunotherapy targeting specific membrane molecules. Nat Med 2011 1712 2011;17:1685–91. https://doi.org/10.1038/nm.2554.

[104] Pereira PMR, Korsak B, Sarmento B, Schneider RJ, Fernandes R, Tomé JPC. Antibodies armed with photosensitizers: from chemical synthesis to

photobiological applications. Org Biomol Chem 2015;13:2518–29. https://doi.org/10.1039/C4OB02334J.
[105] Mesquita MQ, Dias CJ, Gamelas S, Fardilha M, Neves MGPMS, Faustino MAF. An insight on the role of photosensitizer nanocarriers for Photodynamic Therapy. An Acad Bras Cienc 2018;90:1101–30. https://doi.org/10.1590/0001-3765201720170800.
[106] Kou L, Sun J, Zhai Y, He Z. The endocytosis and intracellular fate of nanomedicines: implication for rational design. Asian J Pharm Sci 2013;8:1–10. https://doi.org/10.1016/J.AJPS.2013.07.001.
[107] Hari SK, Gauba A, Shrivastava N, Tripathi RM, Jain SK, Pandey AK. Polymeric micelles and cancer therapy: an ingenious multimodal tumor-targeted drug delivery system. Drug Deliv Transl Res 2023;13:135–63. https://doi.org/10.1007/s13346-022-01197-4.
[108] Wu Y, Wu J, Wong W-Y. A new near-infrared phosphorescent iridium(<scp>iii</scp>) complex conjugated to a xanthene dye for mitochondria-targeted photodynamic therapy. Biomater Sci 2021;9:4843–53. https://doi.org/10.1039/D1BM00128K.
[109] Zheng Y, He L, Zhang D-Y, Tan C-P, Ji L-N, Mao Z-W. Mixed-ligand iridium (<scp>iii</scp>) complexes as photodynamic anticancer agents. Dalton Trans 2017;46:11395–407. https://doi.org/10.1039/C7DT02273E.
[110] Bi X-D, Yang R, Zhou Y-C, Chen D, Li G-K, Guo Y-X, et al. Cyclometalated iridium (III) complexes as high-sensitivity two-photon excited mitochondria dyes and near-infrared photodynamic therapy agents. Inorg Chem 2020;59:14920–31. https://doi.org/10.1021/acs.inorgchem.0c01509.
[111] Sai DL, Lee J, Nguyen DL, Kim Y-P. Tailoring photosensitive ROS for advanced photodynamic therapy. Exp Mol Med 2021;53:495–504. https://doi.org/10.1038/s12276-021-00599-7.
[112] Wang P, Sun S, Ma H, Sun S, Zhao D, Wang S, et al. Treating tumors with minimally invasive therapy: a review. Mater Sci Eng C 2020;108:110198. https://doi.org/10.1016/j.msec.2019.110198.
[113] Liu B, Zhou H, Tan L, Siu KTH, Guan X-Y. Exploring treatment options in cancer: tumor treatment strategies. Signal Transduct Targeted Ther 2024;9:175. https://doi.org/10.1038/s41392-024-01856-7.